High affinity cross-context cellular assays reveal novel protein-protein interactions of peripheral myelin protein of 22 kDa

Stausberg D[1], Moshkovskii S[2,3], Arlt FA[4,5,8], Fledrich R[6], Stassart RM[7], Nave KA[5], Urlaub H[2,3], Ewers D[1,4,9] and Sereda MW[1,4,9]

[1]Research Group Translational Neurogenetics, Max Planck Institute for Multidisciplinary Sciences, Göttingen, Germany
[2]Bioanalytical Mass Spectrometry, Max Planck Institute for Multidisciplinary Sciences, Göttingen, Germany
[3]Bioanalytics, Department of Clinical Chemistry, University Medical Center Göttingen, Göttingen, Germany
[4]Department of Neurology, University Medical Center Göttingen, Göttingen, Germany
[5]Department of Neurogenetics, Max Planck Institute for Multidisciplinary Sciences, Göttingen, Germany
[6]Institute of Anatomy, Medical Faculty, University of Leipzig, Leipzig, Germany
[7]Paul-Flechsig-Institute for Brain Research, Medical Faculty, University of Leipzig, Leipzig, Germany
[8]Present address: Department of Neurology and Experimental Neurology, Charité - Universitätsmedizin Berlin, Berlin, Germany friederike-antonia.arlt@charite.de
[9]These authors contributed equally
E-mail: david.ewers@med.uni-goettingen.de; mwsereda@med.uni-goettingen.de

Keywords: Peripheral myelin protein 22 kDa, Charcot-Marie-Tooth disease 1A, Protein-protein interaction, Immunoprecipitation, Affinity chromatography, Mass spectrometry
Word count: 5,908

Abstract

Peripheral Myelin Protein 22 (PMP22) is a tetraspan membrane protein whose altered dosage causes the most common hereditary neuropathy, Charcot-Marie-Tooth disease type 1A (CMT1A). Despite its clinical significance, the physiological functions of PMP22 and the mechanism behind its tightly controlled gene dosage sensitivity remain unknown since over 30 years, in part due to limited knowledge of its protein-protein interactions (PPIs). In fact, integral membrane proteins such as PMP22 are significantly underrepresented in known cellular interactomes, likely due to limited suitability or technical challenges specific to these hydrophobic molecules in the major PPI discovery approaches. Here, we applied a rigorously optimized co-immunoprecipitation and mass spectrometry workflow using the mild detergent DDM and the high affinity ALFA-tag/anti-ALFA nanobody interaction to identify cellular PMP22-associated proteins. In a cross-context approach, we ran our standardized pipeline across multiple cell types including HEK293T, MDCKII epithelial cells, the Schwann cell line MSC80, and primary rat Schwann cells. We confirm known interactors, and uncover distinct, cell type-specific enrichment patterns following functional annotation analysis. Adhesion-related PPIs dominated in MDCKII cells (e.g., CD47, CLDN1, ATP1B1), while in Schwann cells myelin-associated PPIs were enriched. Importantly, we identified novel PPI candidates that may be highly relevant for PMP22 function including enzymes of the *de novo* sphingolipid biosynthesis pathway.

Introduction

Peripheral Myelin Protein 22 kDa (PMP22) is a small tetraspan transmembrane protein that is predominantly expressed by myelinating Schwann cells (Kitamura *et al*, 1976; Snipes *et al*, 1992; Zanotti *et al*, 2022). *PMP22* has received widespread attention since it was revealed as the disease-causing gene in Charcot-Marie-Tooth disease type 1A (CMT1A), which results from an intrachromosomal gene duplication leading to approximately 1.5-fold overexpression at both the mRNA and protein level (Lupski *et al*, 1991; Raeymaekers *et al*, 1991; Lupski *et al*, 1992; Patel *et al*, 1992; Matsunami *et al*, 1992; Timmerman *et al*, 1992; Valentijn *et al*, 1992; Sereda *et al*, 1996; Li *et al*, 2013; Hertzog & Jacob, 2023). CMT1A, the most prevalent hereditary neuropathy, is characterized by abnormal myelin growth and subsequent axonal loss (Pareyson & Marchesi, 2009; Pisciotta & Shy, 2023). We and others have established abnormal trafficking of the disease protein (Marinko *et al*, 2020) and insufficient differentiation of Schwann cells with dysregulation of (myelin) growth signaling (Fledrich *et al*, 2014, 2019; Fornasari *et al*, 2018; Krauter *et al*, 2024) and lipid metabolism (Vigo *et al*, 2005; Fledrich *et al*, 2012, 2018; Visigalli *et al*, 2020; Zhou *et al*, 2020; Michailidou *et al*, 2023; Capodivento *et al*, 2024; Prior *et al*, 2024), but the normal function of PMP22 and the details of the CMT1A disease mechanism remain largely unclear. Multiple preclinical therapeutic approaches aimed to reduce *PMP22* mRNA levels (Sereda *et al*, 2003; Meyer zu Hörste *et al*, 2007; Chumakov *et al*, 2014; Zhao *et al*, 2018; Prukop *et al*, 2019, 2020; Serfecz *et al*, 2019; Boutary *et al*, 2021, 2025; Gautier *et al*, 2021; Van Lent *et al*, 2023; Yoshioka *et al*, 2023; Espallergues *et al*, 2025). However, the degree of downregulation remains a challenge as the normal dosage window is very narrow, because too little PMP22 (haploinsufficiency) causes hereditary neuropathy with liability to pressure palsies (HNPP) (Adlkofer *et al*, 1995, 1997).

The activation of cellular stress cascades upon misfolding and aggregation of overexpressed PMP22 has been proposed as the primary CMT1A disease mechanism (Notterpek et al., 1999). However, the absence of aggregates and mistrafficking in peripheral nerves of young CMT1A patients (Nishimura *et al*, 1996; Hanemann *et al*, 2000) and suitable CMT1A models (Jouaud *et al*, 2019; Niemann *et al*, 2000) challenge this notion. We note that the PI3K-Akt-mTOR signaling cascade, which is important for myelin growth, is dysregulated in opposite directions in CMT1A and HNPP (Fledrich *et al*, 2014; Krauter *et al*, 2024), although, in the latter, no pathological aggregation should be expected. Thus, gain of a normal function of PMP22 in regulation of myelin biosynthesis seems more likely responsible for the lack of Schwann cell differentiation and subsequent dysmyelination in CMT1A. In line with this scenario, before its role in peripheral myelination was recognized, *PMP22* was discovered as a growth arrest specific gene (*gas3*) in fibroblasts (Schneider *et al*, 1988), and its expression in multiple cell types (Suter *et al*, 1994) and reported roles in progression of various cancers (Winslow *et al*, 2013; Liu & Chen, 2015; Qu *et al*, 2015) suggest a growth-regulatory function of PMP22 in non-myelinating cells.

Protein-protein interactions (PPIs) are essential for the cellular function of most proteins (Stumpf *et al*, 2008; Venkatesan *et al*, 2009; Michaelis *et al*, 2023). PMP22 may thus exert its function(s) both in Schwann cells and other cell types through physical interaction with other proteins, making comprehensive discovery of PMP22's PPIs an important prerequisite for studies aiming to further elucidate its role in health and disease. Several putative PPIs of endogenous PMP22 have already been detected in peripheral nerves using co-immunoprecipitation (Co-IP) (Dickson *et al*, 2002; Amici *et al*, 2006; Guo *et al*, 2014; Hu *et al*, 2016; Vanoye *et al*, 2019; Zhou *et al*, 2019; D'Urso *et al*, 1999), a powerful method to identify direct or indirect interactions. However, the success of Co-IP largely depends on the availability of specific antibodies and, in the case of membrane proteins such as PMP22, on gentle and efficient solubilization from the lipid environment, and these inherent technical challenges may explain previous conflicting results (Amici *et al*, 2006; Poitelon *et al*, 2018). In cultured cells that can be genetically manipulated easily, the specificity problem can be avoided by fusing the protein of interest to epitope- or affinity-tags that can be used to perform Co-IP or affinity purification (AP) under more stringent conditions. Using Co-IP/AP, previously found interactors such as Myelin protein zero (MPZ) (D'Urso *et al*, 1999) and Calnexin (Canx) (Dickson *et al*, 2002) were confirmed (Fontanini *et al*, 2005; Hara *et al*, 2014; Marinko *et al*, 2021; Pashkova *et al*, 2024), and more PPI candidates identified also in non-myelinating cells (Wilson *et al*, 2002; Guo *et al*, 2014; Hara *et al*,

2014; Hu *et al*, 2016; Zhou *et al*, 2019; Marinko *et al*, 2021). Several efforts using Yeast Two-Hybrid (Y2H) screening or Co-IP-mass spectrometry (MS) to reveal PPIs of single proteins or whole interactomes (Wang *et al*, 2011, 2023; Dittmer *et al*, 2014; Rolland *et al*, 2014; Sahni *et al*, 2015; Luck *et al*, 2020; Haenig *et al*, 2020) or specifically PMP22 interactors (Marinko *et al*, 2021) detected further candidate PPIs of PMP22. However, the limited overlap between the previous results indicates that the identified PPIs are far from covering all of PMP22's interaction partners, and few PPIs have been found in Schwann cells so far. To establish a solid foundation for functional studies on the role of PMP22 in both Schwann cells and non-myelinating cells, we used an optimized Co-IP-MS approach that employs a novel epitope tag with high affinity to an engineered nanobody, to generate a comprehensive list of PMP22 interaction candidates in various cell types, including Schwann cells.

Results

To investigate PPIs of PMP22, we used Co-IP-MS from HEK293T (HEK) cells, a strategy that has also been used by Sanders and colleagues (Marinko *et al*, 2021). This easy to transfect cell line that is likely of adrenal origin (Russell *et al*, 1977; Shaw *et al*, 2002; Lin *et al*, 2014) lacks a known functional role of endogenous PMP22. The cell types in which such role has been described show pronounced front-rear (fibroblasts) or apical-basal (epithelial cells, Schwann cells) polarity, while HEK cells remain non-polarized. Thus, HEK cells seem suitable as a model system to investigate basic PPI of PMP22 that are not required for its specialized function in polarized cells. To enable efficient

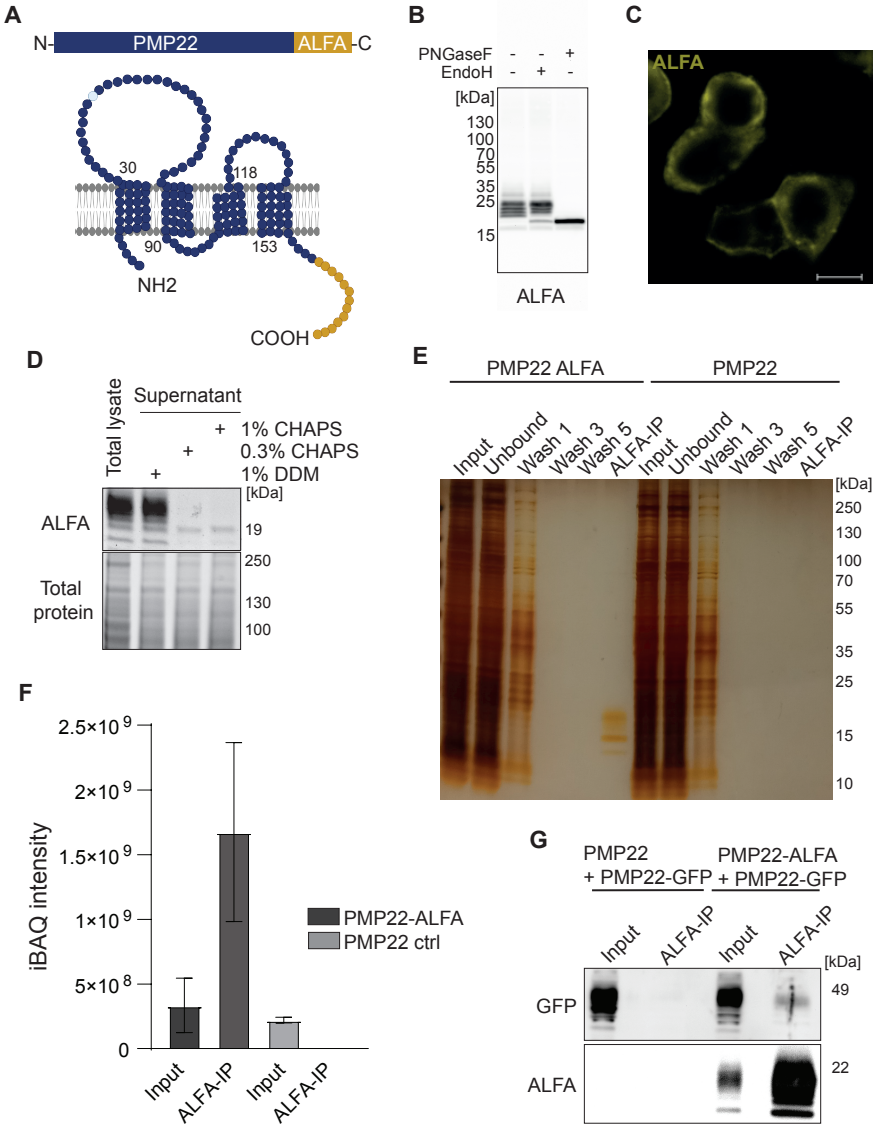

Figure 1. Low-recovery, low-background Co-IP of PMP22 via the ALFA tag. (A) Schematic representation of the PMP22 secondary protein structure with the C-terminal ALFA tag. N-linked glycosylation site at asparagine 41 is highlighted in light blue. (B) Western Blot of HEK cell lysate after PMP22-ALFA transfection subjected to PNGase F and Endo H digestion, showing complex glycosylation of PMP22-ALFA with multiple bands ranging from 19 to 25 kDa. (C) Immunofluorescent staining shows PMP22-ALFA (orange) localized at the plasma membrane in HEK cells. Scale bar is 10 µm. (D) Western Blot analysis of detergent-solubilized PMP22-ALFA comparing solubilization efficiency using 1% DDM, 0.3% CHAPS, and 1% CHAPS. PMP22 was most effectively solubilized by 1% DDM. (E) Silver-stained gel of the PMP22-ALFA Co-IP workflow validating high purity of the PMP22-ALFA eluate in HEK cells. PMP22 transfected HEK cells serve as a control. 9-fold higher amounts of ALFA IP fractions were loaded as compared with input. (F) Chymotrypsin digestion confirms comparable amounts of PMP22-ALFA in the input of the experimental condition and PMP22 in the input of the control, as determined by intensity-based absolute quantification (iBAQ) intensity. Further, it validates the specific enrichment of PMP22-ALFA in the ALFA IP fraction. (G) Co-transfection of PMP22 with PMP22-GFP and PMP22-ALFA with PMP22-GFP confirms PMP22 oligomer formation via Western Blot analysis.

capture of PMP22 in Co-IP, we decided to use the ALFA-tag, which was recently developed by rational design and reported to enable low-background IP by means of the highly specific and high-affinity interaction with anti-ALFA nanobody (Götzke *et al*, 2019). We employed a plasmid that allows expression of C-terminally ALFA-tagged human PMP22 (Fig. 1A) together with a blue fluorescent protein (mTAGBFP2) (Subach *et al*, 2011) driven by a separate promotor to allow for identification of transfected cells via fluorescent microscopy. Following transfection of HEK cells, Western Blot analysis showed ALFA-tag positive bands in the cell lysate that were mostly PNGase F sensitive and Endo H resistant, indicating complex glycosylation after Golgi processing (Fig. 1B). In line with this observation, immunostaining revealed PMP22-ALFA at or near the cell surface (Fig. 1C). Co-IP of membrane proteins requires their efficient extraction from the lipid bilayer with subsequent ultracentrifugation to enable separation from non-interacting, colocalizing proteins. Fig. 1D shows successful solubilization of PMP22-ALFA in all glycosylation states by n-Dodecyl-β-D-maltopyranoside (DDM), a gentle, non-ionic detergent. DDM is known for its superior efficiency in membrane extraction for structural studies (Newstead *et al*, 2008; Stetsenko & Guskov, 2017; Choy *et al*, 2021; Harrison *et al*, 2023; Vénien-Bryan & Fernandes, 2023), and was recently applied in combination with cholesteryl hemisuccinate for successful Co-IP of PMP22 and MPZ (Pashkova *et al*, 2024). Interestingly, that study also reported failure of Co-IP with NP-40 and Triton X-100, two detergents previously used for Co-IP of PMP22 with MPZ and other proteins (Fontanini *et al*, 2005; D'Urso *et al*, 1999). A recent Co-IP-MS study used CHAPS (Marinko *et al*, 2021), a zwitterionic detergent that has been reported to be more efficient in breaking PPIs than NP-40 and Triton X-100 (Labeta *et al*, 1988). To assess its suitability for solubilization of PMP22-ALFA from HEK cell membranes, we tested CHAPS at a concentration of 0.3%, which was used by Sanders and colleagues, as well as at 1%, well above the critical micelle concentration (Chattopadhyay & Harikumar, 1996). Both conditions resulted in extraction of only a small fraction of PMP22-ALFA, specifically of lower molecular weight, while CHAPS failed to solubilize higher molecular weight PMP22-ALFA (Fig. 1D). Unlike DDM, CHAPS therefore seemed not well suited for extracting PMP22-ALFA from the Golgi and the plasma membrane for IP. We thus performed IP using DDM for membrane solubilization and magnetic beads coupled to anti-ALFA nanobody. As inputs we used the supernatant after ultracentrifugation of solubilized HEK cells transiently expressing either PMP22-ALFA or untagged PMP22 as a control. Transfection efficiencies were similar as judged by comparable fluorescence of co-expressed mTAGBFP2 (suppl. Fig. 1). SDS-PAGE with subsequent silver staining showed protein bands resembling PMP22-ALFA in different glycosylation states as previously identified (Fig. 1B) in the eluate of PMP22-ALFA IP, but not of PMP22 IP (Fig. 1E). In line with this observation, label-free quantification (LFQ) MS after chymotrypsin-cleavage detected

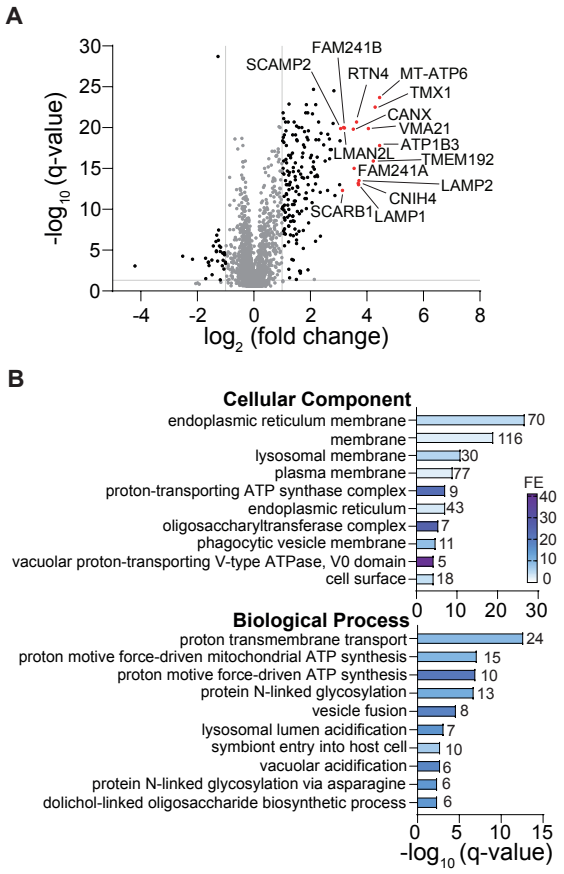

Figure 2. Proteomic and Go-term enrichment analysis of PMP22-ALFA-interactors in HEK cells. (A) Volcano plot of the proteins enriched in PMP22-ALFA IP over background ALFA IP with untagged PMP22. The $\log_2$-transformed fold change is represented on the x-axis, while the $-\log_{10}$-transformed q-value is plotted on the y-axis. The top 15 most enriched proteins in the PMP22-ALFA IP are highlighted in red. Grey lines indicate a $-\log_{10}$-transformed q-value cutoff of 1.301 (corresponding to a q-value of 0.05) and a $\log_2$ fold change threshold of 1, establishing the significance criteria for differential enrichment. Proteins that do not meet these thresholds are displayed in grey. (B) Functional annotation analysis of the enriched proteins for Cellular Compartment and Biological Process aspects. A q-value threshold of <0.05 was used to determine significance. The gene count and fold enrichment (FE) values are shown, with the top 10 most significantly enriched terms presented for each category. The experiment was performed on three experimental replicates and two technical replicates.

similar abundance of PMP22 in both inputs and showed enrichment of PMP22 in the PMP22-ALFA IP eluate, while PMP22 was absent from the IP eluate of untagged PMP22 control (Fig. 1F). PMP22 was previously reported to form homo-oligomers (Tobler *et al*, 1999; Mobley *et al*, 2007). To test the Co-IP approach for successful enrichment of a known, probably directly interacting protein, we thus performed PMP22-ALFA IP following co-transfection of HEK cells with a C-terminal fusion of PMP22 with a monomeric GFP. Indeed, we detected PMP22-GFP via Western Blot analysis in the PMP22-ALFA eluate but not in the negative control, demonstrating self-interaction of PMP22 in HEK cell membranes (Fig. 1G).

We then extended the LFQ-MS analysis to identify PMP22 interactors. Whereas chymotrypsin cleavage can facilitate detection of hydrophobic proteins with few trypsin cleavage sites such as PMP22 (Fischer & Poetsch, 2006), trypsin is better suited for enhanced protein coverage (Dau *et al*, 2020), and we therefore used trypsin as a protease for the remaining experiments. As expected for successful Co-IP, the resulting volcano plot was skewed, showing enrichment of multiple proteins in the PMP22-ALFA eluate compared with the untagged PMP22 background, while only few were depleted (Fig. 2A). The top enriched proteins included previously reported PMP22 interactors, among which were ER resident proteins involved in ER quality control such as Calnexin (CANX) (Dickson *et al*, 2002; Hara *et al*, 2014; Marinko *et al*, 2021) or protein disulfide-isomerase TMX1 (Luck *et al*, 2020), as well as the L-type lectin VIPL (LMAN2L) related to the previously reported interacting ERGIC-53 (LMAN1) (Marinko *et al*, 2021), both of which act as sorting receptors for ER export of transmembrane proteins. However, also proteins localized to the distal part of the secretory pathway where highly enriched, such as the lysosomal LAMP1, LAMP2 and TMEM192, the trans-Golgi recycling carrier Secretory carrier-associated membrane protein 2 (SCAMP2) as well as plasma membrane-localized Na^+/K^+-ATPase subunit beta-3 (ATP1B3) and Scavenger receptor class B member 1 (SCARB1). Functional annotation enrichment analysis of all potential interactors using the Gene Ontology aspect *Cellular Component* confirmed a balanced distribution across the intracellular organelles and the plasma membrane (Fig. 2B). In contrast, only a small fraction of the PPIs reported by Sanders and colleagues are with proteins with reported location at the plasma membrane (Marinko *et al*, 2021) (Suppl. Table 1). Similar to the results of Sanders and colleagues, functional annotation analysis according to *Biological Process* showed enrichment of proteins involved in processing and transport of proteins along the secretory pathway (Fig. 2B).

In Schwann cells, PMP22 plays a still somewhat ill-defined role as an adhesion protein in compact myelin (Pashkova *et al*, 2024; D'Urso *et al*, 1999) as well as in tight and adherens junctions of non-compact myelin (Guo *et al*, 2014; Hu *et al*, 2016). Moreover, an impact of PMP22 on integrin-mediated adhesion to the extracellular matrix (ECM) has been reported in Schwann cells (Amici *et al*, 2006;

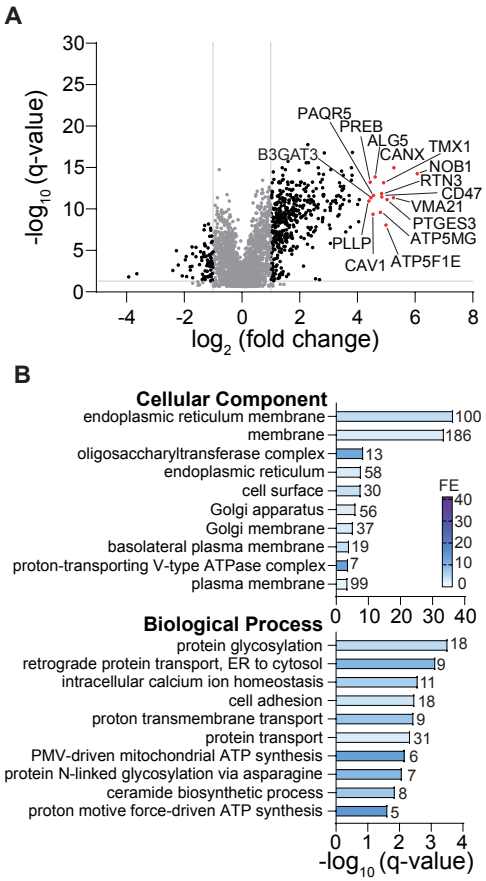

Figure 3. Proteomic and Go-term enrichment analysis of PMP22-ALFA-interactors in MDCKII cells. (A) Volcano plot of the proteins enriched in PMP22-ALFA IP over background ALFA IP with untagged PMP22. The log_2-transformed fold change is represented on the x-axis, while the $-log_{10}$-transformed q-value is plotted on the y-axis. The top 15 most enriched proteins in the PMP22-ALFA IP are highlighted in red. Grey lines indicate a $-log_{10}$-transformed q-value cutoff of 1.301 (corresponding to a q-value of 0.05) and a log_2 fold change threshold of 1, establishing the significance criteria for differential enrichment. Proteins that do not meet these thresholds are displayed in grey. (B) Functional annotation analysis of the enriched proteins for Cellular Compartment and Biological Process aspects. A q-value threshold of <0.05 was used to determine significance. The gene count and fold enrichment (FE) values are shown, with the top 10 most significantly enriched terms presented for each category. The experiment was performed on three experimental replicates and two technical replicates.

Poitelon *et al*, 2018) and other cells (Brancolini *et al*, 1999; Rao *et al*, 2011). Beyond Schwann cells in peripheral nerves, *PMP22* also shows relatively strong expression in various epithelia (Baechner *et al*, 1995; Roux *et al*, 2004) and has been shown to contribute to intercellular adhesion in the epithelial Madin-Darby Canine Kidney (MDCKII) cell line (Notterpek *et al*, 2001; Roux *et al*, 2005; Zoltewicz *et al*, 2012). Several PPIs of PMP22 related to a function in extracellular and autotypic adhesion have been reported (Amici *et al*, 2006; Guo *et al*, 2014; Hu *et al*, 2016; Pashkova *et al*, 2024). We reasoned that Co-IP-MS from MDCKII cells is suitable for discovering interaction partners of PMP22-ALFA that are related to such specialized functions as cellular adhesion. Fig. 3A shows that indeed CD47, a plasma membrane localized protein involved in integrin-mediated adhesion (Wang *et al*, 1999; Reed *et al*, 2019) and previously reported as a peripheral myelin protein (Gitik *et al*, 2011; Siems *et al*, 2020), is among the highest enriched proteins in MDCKII cells. Functional annotation analysis according to *Biological Process* further shows the term *cell adhesion* highly enriched (Fig. 3B), the most enriched PPI candidates in the PMP22-ALFA eluate of this group being CD47, the beta 1 subunit of the Na^+/K^+-ATPase (ATP1B1), which has a crucial function in the formation of adherens junctions (Vagin *et al*, 2006), the important tight junction component Claudin 1 (CLDN1) (Furuse *et al*, 1998) as well as CD44, which mediates cell-ECM interactions via binding various ECM components (Dzwonek & Wilczyński, 2015). According to the enrichment of PPI candidates associated with cell-ECM and intercellular adhesion, the *Cellular Component* terms *cell surface* and *basolateral plasma membrane* were enriched (Fig. 3B). In addition, the PMP22-ALFA eluate showed enrichment of several proteins involved in biosynthesis of the essential myelin lipid class of sphingolipids, reflected in enrichment of the term *ceramide biosynthetic process* in the functional annotation aspect *Biological Process*s (Fig. 3B). Among the proteins in this group are the ceramide synthases CERS2 and CERS6, as well as all three isoforms of serine palmitoyltransferase (SPTLC1,2,3), the pacemaker enzyme in the *de novo* sphingolipid synthesis pathway (Quinville *et al*, 2021). Moreover, two isoforms of a regulatory protein (ORMDL2,3) and two further enzymes involved in sphingolipid synthesis, 3-ketodihydrosphingosine reductase (KDSR) and dihydroceramide desaturase (DEGS1), were enriched in the PMP22-ALFA eluate. Interestingly, among the top 15 most enriched proteins in the PMP22-ALFA eluate were Caveolin 1 (CAV1), which is crucial for formation of the cholesterol and sphingolipid sequestering caveolae (Örtegren *et al*, 2004; Ariotti *et al*, 2014), as well as Plasmolipin (PLLP), a tetraspan, highly abundant myelin protein in both the central and the peripheral nervous system that contains a sphingolipid binding domain and plays a role in myelin biogenesis by myelin precursor membrane formation in the secretory pathway (Bosse *et al*, 2003; Yaffe *et al*, 2015; Azzaz *et al*, 2023). Considering PMP22's proposed role in regulation of myelin lipid metabolism (Stefanski *et al*, 2024; Silva *et al*, 2025), these novel PMP22 PPI candidates are of particular interest.

PMP22 plays its most significant role in myelinating Schwann cells, reflected in the striking PMP22 dose sensitivity leading to both CMT1A and HNPP. To discover new PPI candidates in Schwann cells, we turned to MSC80, an immortalized cell line derived from secondary, peripheral nerve cell culture that retained important characteristics like Schwann cell morphology and expression of Schwann cell markers (Boutry *et al*, 1992). Importantly, MSC80 cells were able to myelinate injured axons after transplantation *in vivo* (Boutry *et al*, 1992). We treated the cells with cyclic AMP analog dbcAMP to stimulate upregulated expression of myelination related genes (Brockes *et al*, 1979; Arthur-Farraj *et al*, 2011). However, after 24 hours of dbcAMP treatment, at the proteomic level we were unable to detect any switch to a pro-myelinating expression signature (suppl. Fig. 2), which may reflect a limitation of this cell line as a Schwann cell model. Nonetheless, in stimulated MSC80 cells, several of the top 15 PPIs (Fig. 4A) candidates have previously been reported as peripheral myelin proteins (Siems *et al*, 2020), including, interestingly, those primarily associated with cellular energy regeneration in mitochondria (ATP5F1B, ATP5F1D, ATP5MF) or protein glycosylation in the ER (DDOST, RPN1). However, many canonical proteins of the myelin sheath were also found among the enriched proteins in the PMP22-ALFA eluate, including the established PMP22 interaction partner MPZ (Pashkova *et al*, 2024), the proteolipid protein (PLP1), the Rho-type GTPase cell division cycle 42 (CDC42), Cell surface glycoprotein MUC18 (MCAM) as well as several Annexin isoforms (ANXA1,2,5,6) (Shih *et al*, 1998; Benninger *et al*, 2007; Hayashi *et al*, 2007; Siems *et al*, 2020) (Fig. 4A). In line with these observations, functional annotation analysis showed enrichment of the *Cellular Component* term *myelin sheath* (Fig. 4B). Moreover, like in MDCKII cells (Fig. 3) proteins involved in

sphingolipid synthesis such as SPTLC1, SPTLC2, CERS2 and KDSR were again enriched among the PMP22 PPI candidates (Fig. 4B).

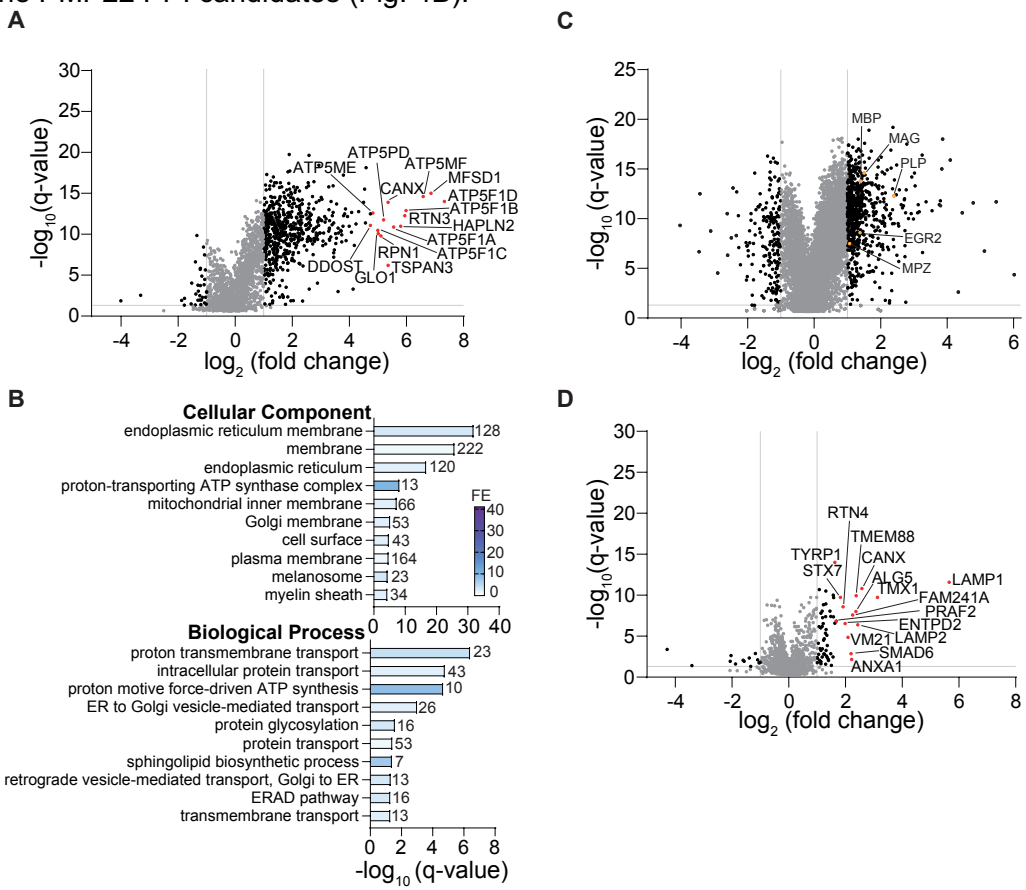

Figure 4. Proteomic and Go-term enrichment analysis of PMP22-ALFA interactors in Schwann cells. (A) Volcano plot of proteins identified in PMP22-ALFA IP from MSC80 cells, compared to control IP with untagged PMP22. The top 15 enriched proteins are highlighted in red. (B) Functional annotation analysis of proteins enriched in the PMP22-ALFA IP from MSC80 cells, covering the categories Cellular Compartment and Biological Process. The top 10 significantly enriched terms ($q < 0.1$) are shown with gene counts and fold enrichment (FE) values. (C) Differential proteome analysis of primary Schwann cells under unstimulated and cAMP-stimulated conditions. Key myelin proteins (MBP, MAG, PLP, EGR2, MPZ) are highlighted in orange. (D) Volcano plots of proteins identified in PMP22-ALFA IP from stimulated primary Schwann cells, compared to control IP with untagged PMP22. Volcano plots display $\log_2$ fold change on the x-axis versus $-\log_{10}$ q-value on the y-axis. Grey lines indicate the thresholds for significant enrichment ($q < 0.05$; $\log_2$ fold change > 1). Proteins not meeting these criteria are shown in grey. All experiments were performed in three biological and two technical replicates.

We then turned to primary Schwann cells isolated from peripheral nerves of rats at postnatal day (P) 2-P4 since we expected primary Schwann cells to be more readily stimulated towards a differentiated phenotype than the MSC80 cell line. Indeed, upon dbcAMP treatment, we found the pro-myelinating transcription factor Krox20 (EGR2) together with major myelin proteins upregulated on the protein level (Fig. 4C). However, as compared with the previously investigated cell types, transient transfection was only successful in a smaller fraction of primary Schwann cells (suppl. Fig. 1D, D'). Thus, probably due to high background from non-transfected cells contributing to the Co-IP input, we found considerably less (63) proteins that were enriched in the PMP22-ALFA eluate (Fig. 4D, Fig. 5A), and functional annotation did not show any significant enrichment. Despite the considerably lower number of PPI candidates that resulted from primary Schwann cells as compared to other cell types, we again found multiple reported myelin proteins including those that we found in MSC80 cells, such as MPZ, PLP1, MCAM and ANXA1. The Venn diagram in Fig. 5A shows the overlap of all PPI candidates shown in Figs. 2-4, and Fig. 5B lists all PPI candidates that were found at least in two cell types.

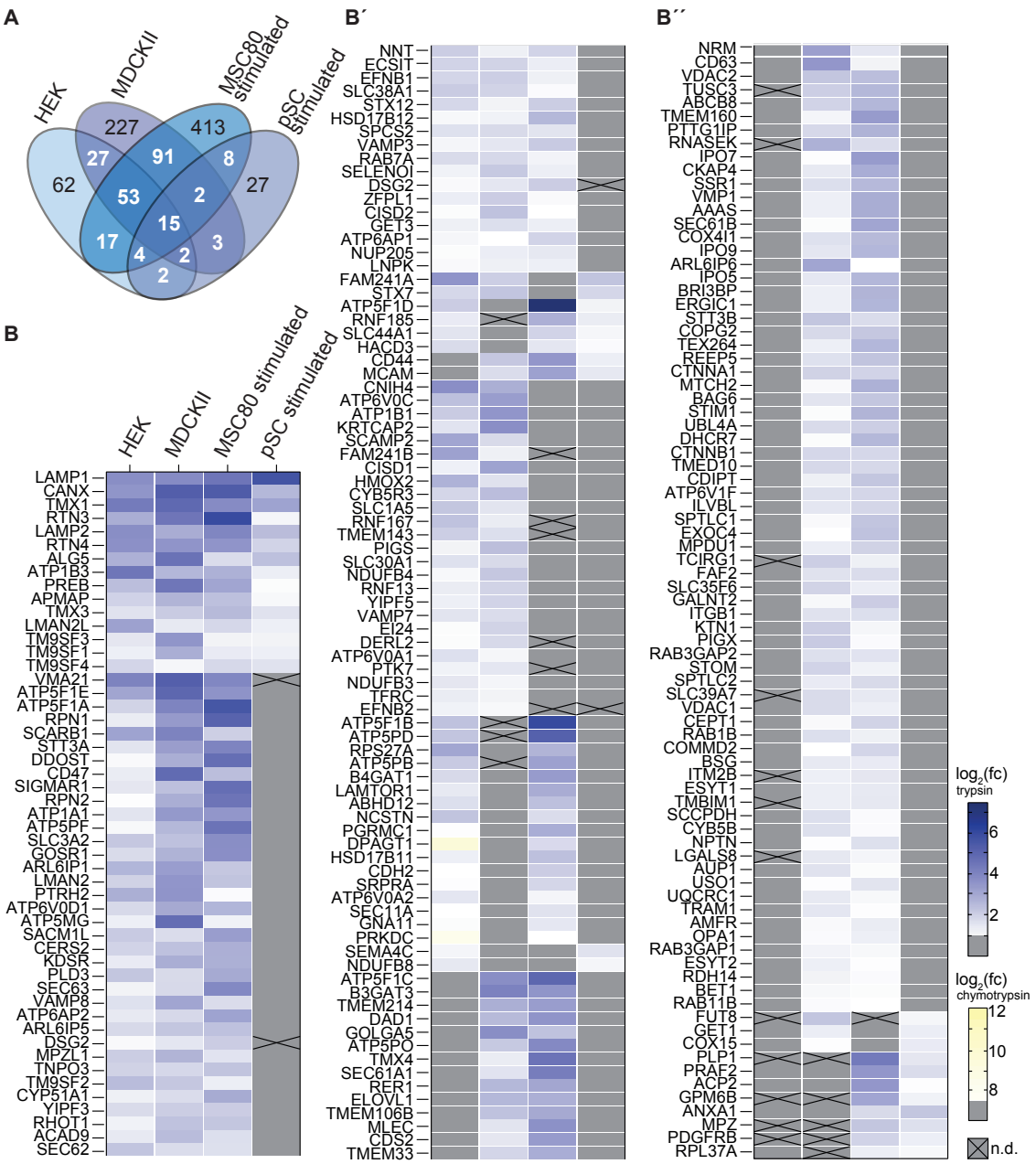

Figure 5. Comparison of PMP22-ALFA PPIs across cell types and conditions. (A) Venn diagram illustrating the overlap of identified proteins across four PMP22 ALFA Co-IP conditions, considering proteins with a q-value below 0.05 and a $\log_2$-transformed fold change >1. The four groups analyzed are HEK cells, MDCKII cells, stimulated MSC80 and primary Schwann cells (pSC). (B), (B´) and (B´´) List of proteins identified in the Co-IP experiments including those detected in at least two of the cell types/conditions, with a q-value below 0.05. The heat map represents the $\log_2$ fold change of each protein relative to the control, with values indicated by shades of blue (trypsin digestion) or yellow (chymotrypsin digestion, shown for proteins that were not detected after trypsin digestion). Grey indicates that the protein was not detected or did not meet the cutoff criteria of enrichment in the ALFA-IP, while a cross denotes that it was also not detected in the respective input sample.

Discussion

The aim of this study was to identify novel PPIs of PMP22, with a view to providing a basis for further, functional investigations. We employed a Co-IP approach combining the optimized, efficient and gentle removal of PMP22 from its native environment in various cellular membrane compartments including the plasma membrane, with a highly specific, high-affinity epitope-nanobody pair. This allowed 1,074 new candidates to be added and confirming 54 of the existing—to our knowledge—296 PMP22 candidate PPIs (suppl. Table 2). In the extensive data available on the interactome of eukaryotic cells derived from the most successful techniques for large-scale PPI discovery, Y2H and

AP-MS/IP-MS, PPIs of membrane proteins are underrepresented, due to various biological and technical challenges such as misfolding and subcellular localization as well as insufficient solubilization (Sharifi Tabar *et al*, 2022). It is therefore not surprising that the PPIs of PMP22 that have been discovered using these techniques to date are relatively few compared to our results (Wang *et al*, 2011, 2023; Dittmer *et al*, 2014; Rolland *et al*, 2014; Sahni *et al*, 2015; Luck *et al*, 2020; Marinko *et al*, 2021; Haenig *et al*, 2020). Through efficient solubilization of PMP22, most likely this study was the first to enable sampling of its PPIs in all cellular membrane compartments. Thus, besides intracellular compartments like ER and Golgi, in functional annotation analysis we found a significant fraction of PPI candidates localized at the cell surface (Figs. 2B, 3B, 4B), including specialized plasma membrane compartments like the basolateral membrane of MDCKII cells where intercellular junctions are formed (Fig. 3B). In the Schwann cell line MSC80 we found the term myelin sheath enriched (Fig. 4B), with several known myelin proteins like PLP1, MPZ, MCAM and ANXA1 enriched in the PMP22-ALFA eluates of MSC80 and primary Schwann cells. At the onset of myelination, Schwann cells mount a transcriptional program enabling coordinated synthesis of both myelin proteins and lipids that are required in large quantities for myelin sheath formation (LeBlanc *et al*, 2005; Pertusa *et al*, 2007; Fledrich *et al*, 2018; Kim *et al*, 2018; Poitelon *et al*, 2020). In recent years, evidence has accumulated that links PMP22 to lipid metabolism and importantly, dysregulation of lipid synthesis and transport to PMP22-related neuropathies, most severely affecting the major myelin sterol lipid cholesterol as well as the lipid class of sphingolipids (Fledrich *et al*, 2012, 2018; Zhou *et al*, 2019; Visigalli *et al*, 2020; Michailidou *et al*, 2023; Prior *et al*, 2024; Capodivento *et al*, 2024; Zhou *et al*, 2020). Strikingly, both in polarized epithelial cells and in Schwann cells, we here detected interaction of PMP22 with the sphingolipid synthesis machinery of the ER. The initial step of the *de novo* sphingolipid synthesis pathway is catalyzed by the serine palmitoyltransferase complex (SPT), a homo-dimeric assembly of a hetero-tetramer that consists of the enzyme core (SPTLC1 and SPTLC2 or SPTLC3) and two transmembrane accessory subunits (ORMDL1,2 or 3 and serine palmitoyltransferase small subunit (SPTSS) A or B) (Li *et al*, 2021; Wang *et al*, 2021). All SPT subunits resulted as PMP22 PPI candidates but SPTSSA and SPTSSB, which are only 71 or 76 amino acids in length and feature unfavorable tryptic cleavage sites for detection via MS. Accordingly, we could not detect the small subunits in any of the Co-IP input samples. Of note, Co-IP from cell lysates results in enrichment of both direct and indirect interactors, and interaction with just one of the subunits of a stable complex can thus suffice to detect all subunits. To our knowledge, there is no evidence so far that the remaining enzymes of the *de novo* sphingolipid synthesis pathway (CERS, KDSR, DEGS) interact with SPT, so they may operate separately. Since in addition to SPT, we identified all three as PPI candidates, it seems likely that PMP22 can directly interfere with sphingolipid synthesis in the ER, with a possible functional role of contributing to physiological regulation of sphingolipid supply to the myelin sheath and to its dysregulation in CMT1A. PPIs resulting from Co-IP-MS inevitably contain false positives due to contaminants or background noise (Dunham *et al*, 2012). Therefore, our PPI results cannot be considered valid on their own. Instead, when used as input for future candidate or functional screening studies, PPI candidates will have to be validated using orthogonal technical approaches. These might include techniques providing evidence of physical interaction like crosslinking MS (Larance *et al*, 2016; Leitner *et al*, 2016; O'Reilly & Rappsilber, 2018; Piersimoni *et al*, 2022) or more direct methods that require purified proteins like surface plasmon resonance (Puiu & Bala, 2016). Proximity of PMP22 and PPI candidates *in-situ* may be tested using techniques that also provide information about the subcellular location of PPI, like Proximity ligation in fixed cells (Söderberg *et al*, 2006) or FRET/BRET assays in living cells (Machleidt *et al*, 2015). In light of the dosage effect of PMP22, we also note that transient overexpression can be expected to result in considerable alterations in its PPIs. Moreover, by restricting our approach to monoculture *in vitro*, we certainly have missed those interactions of PMP22 that require the cellular architecture of myelinating Schwann cells *in vivo*. Future investigations employing DNA-editing approaches may be able to sample the entirety of PMP22's PPIs, at endogenous expression levels within the developing axon-Schwann cell unit. Nevertheless, in this study we were able to significantly expand the range of potential interaction partners of PMP22, thereby creating new, evidence-based starting points for future studies. Given that there is still no therapy available in CMT1A, the identification of new PPIs may thus form a new family of future therapeutic targets for PMP22-associated diseases.

Methods

Cell culture

HEK293T cells (MERCK, #96121229) and MSC80 cells (Boutry et al., 1992) were cultured in DMEM (Gibco, Thermo Fisher) supplemented with 10% FCS (Gibco, Thermo Fisher) and 1% penicillin/streptomycin (Pen/Strep (Lonza)) while MDCKII cells (Merck, #00062107) were maintained in MEM medium (Gibco, Thermo Fisher), supplemented with 5% FCS and 1% Pen/Strep.
Primary Schwann cell monocultures were prepared from rats at P2-P4. Dissected sciatic nerves of six rats were pooled and enzymatically digested with trypsin (Invitrogen, Thermo Fisher) and collagenase II (Worthington) for 1 hour at 37 °C. The tissue was dissociated by triturating and the reaction stopped by adding 25% FCS in basic medium (DMEM). Cells were plated in Schwann cell basic medium (1% Pen/Strep, 10% FCS, 1% GlutaMax (Gibco, Thermo Fisher)) on PLL-coated culture plates. The following day fibroblasts were eliminated by supplementing the medium with 10 µM Cytosine β-D-arabinofuranoside hydrochloride (AraC (Sigma)) for 2 days. Primary Schwann cells were stimulated for 24 hours with 2 mM dbcAMP (BIOLOG) in the presence of 5% FCS, control cells were maintained in growth medium containing 5% FCS for this incubation period.
HEK293T cells were transiently transfected with ALFA-, GFP-, or untagged PMP22 expression plasmids (VectorBuilder) using polyethylenimine (Polysciences, Inc), while MDCKII, MSC80, and primary Schwann cells were transfected via Lipofectamine™ 3000 (Thermo Fisher).

Cell lysates

Cell pellets from one transfected 10 cm plate were resuspended in ice-cold TBS buffer (100 mM Tris/HCl, 150 mM NaCl, pH 7.5) supplemented with a complete protease inhibitor cocktail (Roche Diagnostics). To compare optimal detergents for analysis, samples were incubated for 1 hour at RT with either 1% CHAPS (AppliChem), 0.3% CHAPS, or 1% DDM (Anatrace), followed by centrifugation at 100,000 × g for 1 hour at 4 °C.

Co-IP

DDM-solubilized cell lysate was diluted with TBS to a final concentration of 0.15% DDM. Insoluble material was pelleted via centrifugation at 100,000 × g for 1 hour at 4 °C. Protein concentrations were determined with the Bio-Rad DC™ Protein Assay Kit and adjusted. Magnetic ALFA Selector PE Resin beads were washed and equilibrated before adding the cleared cell lysate. After incubation for 90 minutes at 4 °C, the beads were washed six times with cold TBS buffer containing 0.025% DDM. PMP22-ALFA was then eluted by providing an excess of ALFA peptide.

Glycosylation assay

Cleared cell lysates were treated with Endoglycosidase (Endo) H and Peptide N-Glycosidase (PNGase) F (New England Biolabs) according to the manufacturer's instructions, and the proteins were evaluated by Western blotting with peroxidase-conjugated anti-ALFA antibody.

SDS Page and Western Blotting

Proteins were separated by electrophoresis using 4–20% precast polyacrylamide gels (Novex™ Tris-Glycin Mini gels, Thermo Fisher). PageRuler Plus Prestained Protein Ladder (Thermo Fisher) was used for loading and size control. The proteins were then transferred to a methanol-activated PVDF membrane (Immobilon-P Membrane; Millipore, Merck). Fast Green staining was performed to determine the total protein load. Therefore, membranes were rinsed in Fast Green washing solution (30% methanol, 6.7% glacial acetic acid) to remove transfer buffer residues and then incubated in Fast Green staining solution (0.5% Fast Green (Sigma), 30% methanol, 6.7% glacial acetic acid) for 5 minutes. The membranes were then washed twice in Fast Green washing solution before fluorescent imaging using the ChemoStar imager (INTAS Science Imaging Instruments). Membranes were blocked in milk-TBST (5% milk powder, 25 mM Tris, 75 mM NaCl, 0,05 % Tween 20) for 1 hour at room temperature, and then incubated overnight at 4 °C with primary antibodies (sdAB ALFA-HRP 1:40000; NanoTag Biotechnologies N1501 #15201101; GFP 1:1000, Abcam #ab290), diluted in

blocking solution. After 5–7 washing steps with TBST, membranes were incubated, when required, with HRP-conjugated secondary antibodies (1:20000, Dianova), for 2 hours at room temperature, followed by additional washes and detection using the Western Lightning Plus ECL Kit.

Silver staining

For silver staining, gels were fixed overnight in 40% ethanol and 10% acetic acid. The next day the gels were washed twice for 20 minutes in 20% ethanol, and once for 20 minutes in ddH_2O. Pretreatment was performed for 1 minute in 0.8 mM sodium thiosulfate, followed by three 20 seconds washes in ddH_2O. Gels were then stained for 20 minutes in 0.2% silver nitrate containing 0.02% formaldehyde and washed again three times for 20 seconds in ddH_2O. Protein bands were developed in 3% sodium carbonate with 0.02% formaldehyde until clearly visible, and the reaction was stopped by two 10 minutes incubations in 5% acetic acid.

Immunofluorescence

PMP22-ALFA transfected HEK293T cells were fixed in 4% PFA, washed three times with PBS, and permeabilized in ice-cold methanol/acetone (95% / 5%) for 5 minutes, following another washing series of three times with PBS. Coverslips were placed on blocking solution (2% horse serum (Gibco, Thermo Fisher), 2% BSA (BioMol), 0.1% gelatine) and incubated for 1 hour. Coverslips were incubated overnight at 4 °C with the primary antibody (ALFA polyclonal, 1:500; NanoTag Biotechnologies, N1581 #082312) diluted in blocking solution. Following this, the coverslips were washed three times with PBS and incubated with secondary antibodies (1:1000) for 1 hour at room temperature. After another set of washes, coverslips were mounted onto microscopic slides and imaged using the Zeiss Axio Imager Z1 microscope.

Sample preparation for proteomic analysis

HEK293T, MSC80, and MDCKII cells, as well as primary rat Schwann cells were lysed and in-solution digested by trypsin followed by the data independent acquisition (DIA) proteomic pipeline.

Samples of lysed cells or eluates from ALFA beads were digested by trypsin and cleaned up using SP3 paramagnetic bead protocol (Hughes *et al*, 2019). Briefly, 50 µL of lysates or eluates containing approximately 15 µg total protein was mixed 1:1 (v/v) with 50 mM ammonia bicarbonate and incubated for 10 min at 37°C and 900 rpm shaking. The disulfide bonds were reduced with 10 mM DTT for 30min at 37°*C* and 900 rpm followed by alkylation with 40 mM iodoacetamide (IAA) for 30 min at 25°C and 900 rpm and quenching of the alkylating agent with 10 mM DTT for additional 10 min at *25*°C and 900 rpm. The SP3 beads (PreOmics) were prepared and the samples were bound to the beads as described before using a magnetic rack for Eppendorf tubes. Samples were pre-digested by Benzonase (Universal Nuclease for Cell Lysis, 100kU, Pierce) for 1h at 37°C and 1000 rpm and then by trypsin (Sequencing Grade Trypsin, Promega) in 1:50 w/w ratio to protein overnight at 37°C and 1000 rpm. Tryptic peptides were eluted from the beads according to the SP3 protocol and the resultant eluates were dried in the vacuum concentrator (Eppendorf). Dried samples were redissolved in 0.1% (v/v) formic acid and 2% (v/v) acetonitrile solution. For each run of LC-MS/MS analysis, 100 ng of total protein was injected as measured in lysates before trypsin digestion.

For DIA pipeline, samples were analyzed in 3 technical replicates in each group of samples (PMP22 transfected and control input cells and corresponding IP eluates) and in 2 measurement replicates for each technical replicate.

Since the protein of interest, PMP22, has a low amount of trypsin digestion sites which leads to formation of few long peptides with low detection levels in LC-MS/MS, HEK293T sample set was digested by chymotrypsin followed by the data dependent acquisition (DDA) proteomic pipeline. Input and IP eluate samples were separated by conventional SDS-PAGE in triplicates. Each line was cut into equal 23 slices and the slices were in-gel digested by chymotrypsin (sequencing grade, Promega) as described earlier (Shevchenko *et al*, 1996) .

LC-MS/MS analysis (DIA pipeline)

Nano-HPLC was performed using Dionex UltiMate 3000 chromatographer, where LC effluent solutions were Buffer A (0.1% (v) formic acid) and Buffer B (80% (v) ACN, 0.08% (v) formic acid).

The columns used in LC were the Trap column (PEPMAP100 C18, 0.3 x 5 mm, 5 µm, Thermo) and the main column (Aurora CSI C18, 25 cm x 75 µm, 1.6 µm; IonOpticks). HPLC was performed under a column temperature of 50°C. The solution gradient was as follows: 0-3.5 min 0.4 µL/min 5% (v) buffer B, 3.5-5 min 0.4-0.2 µL/min 5-10% B, 5-40 min 0.2 µL/min 10-42% B, 40-41 min 0.2 µL/min 42-95% B, 41-45 min 0.2 µL/min 95% B, 45-45.5 min 0.2-0.4 µL/min 95-5% B, 45.5-50 min 0.4 µL/min 5% B, where the flow and % buffer B were changing linearly.
The chromatographer was coupled with timsTOF Pro 2 mass spectrometer (Bruker Daltonics). The applied ionization method was nanoelectrospray (Bruker CaptiveSpray) with positive ionization polarity where the capillary voltage was 1.5 kV and dry gas flow rate was 3 L/min. Ionization took place at 180 °C. The TIMS chamber was filled with nitrogen gas at 305 K temperature. The pressure at the tunnel entrance was ~2.7 mbar.
For data-independent acquisition in dia-PASEF high-sensitivity mode (the default method provided by the vendor), an ion mobility range was sampled from 1/K0 1.43 to 0.6 Vs/cm2 using equal ion accumulation and ramp times in the dual TIMS analyzer of 100 ms each. The collision energy was lowered as a function of increasing ion mobility from 59 eV at 1/K0 1.43 Vs/cm2 to 20 eV at 1/K0 0.6 Vs/cm2. Overall, 16 PASEF scans were used with two mass windows per the scan.
The MS and TIMS were calibrated linearly using three ions from the Agilent ESI LC/MS tuning mix (m/z, 1/K0: 622.0289 Th, 0.9915 $V \cdot s \cdot cm^{-2}$; 922.0097 Th, 1.1986 $V \cdot s \cdot cm^{-2}$; 1221.9906 Th, 1.3934 $V \cdot s \cdot cm^{-2}$) in positive mode.

LC-MS/MS analysis (DDA pipeline)
Peptides after in-gel digestion of chymotrypsin were loaded onto nano-HPLC (Dionex Ultimate 3000 UHPLC Thermo Fischer Scientific) coupled with in-house packed C18 column (ReproSil-Pur 120 C18-AQ, 3 µm particle size, 75 µm inner diameter, 30 cm length, Dr. Maisch GmbH). The peptides were separated with a linear gradient of 11–40% buffer B (80% acetonitrile and 0.1% formic acid) at flow rate of 300 nL/min over 37 min gradient time at overall method duration of 58 min. Eluting peptides were analysed by Orbitrap Exploris 480 mass spectrometer (Thermo Fischer Scientific). The following MS settings were used: MS1 scan range, 350–1400 m/z; MS1 resolution, 60,000 FWHM; AGC target MS1, custom; maximum injection time MS1, custom; intensity threshold, 1E4; isolation window, 1.6 Th; normalized collision energy, 28%; charge states, 2+ to 6+; dynamic exclusion, custom; top 20 most abundant precursors were selected for fragmentation; MS2 resolution, 15,000, AGC target MS2, custom; maximum injection time MS2, custom.

LC-MS/MS data processing (DIA pipeline)
Quantitative analysis of proteins from DIA LC-MS/MS runs was done using Spectronaut software (version 19.6.250122.62635, Biognosys) in directDIA mode with default parameters except data imputation which was on with a “background signal” option. Search databases represented reference proteome fasta files downloaded from Uniprot (Bateman *et al*, 2025): human (UP000005640, 2024-02-20), dog (UP000805418, 2024-12-04), rat (UP000002494, 2025-01-22), mouse (UP000000589, 2025-07-16).

LC-MS/MS data processing (DDA pipeline)
Data were processed by MaxQuant (v. 1.6.17.0) (Cox & Mann, 2008) with default parameters for DDA except chymotrypsin as a protease. iBAQ values were used for protein quantitation. Differentially expressed proteins were identified using DEP2 R package (Feng *et al*, 2023).

PPI and functional annotation enrichment analysis
The following criteria were utilized to determine potential PMP22-ALFA interacting proteins. A false discovery rate (FDR)-corrected q-value of less than 0.05 was applied to define significant changes in protein abundance. Only proteins that showed a >1 log2 fold increase in abundance between PMP22-ALFA and control IP samples were considered. To exclude background effects, proteins with a log2 fold change >0.58 (1.5-fold) in the corresponding input samples were removed. Functional enrichment of proteins was performed using DAVID (Database for Annotation, Visualization, and Integrated Discovery)(Sherman *et al*, 2022; Huang *et al*, 2009). UniProt IDs of PMP22 PPI candidates

were submitted to DAVID, with input proteins serving as the background. To ensure specificity, enrichment and analysis was carried out utilizing the GO Direct category.

Data availability
The mass-spectrometry data generated for this study are deposited in the MassIVE repository and submitted to ProteomeXchange Consortium (Deutsch *et al*, 2023) and are available using the following identifiers MSV000099338 (MassIVE), PXD069006 (ProteomeXchange).

Acknowledgments

H.U. was funded by the Deutsche Forschungsgemeinschaft (DFG) SFB1565 (project P04, project number 469281184). K.A.N. was funded by the DFG (NA 262/3-1). M.W.S. was funded by the DFG (SE 1944/3-1). The authors thank Annika Reinelt (Bioanalytical Mass Spectrometry, Max Planck Institute for Multidisciplinary Sciences), Michael Kothe (Department of Neurogenetics, Max Planck Institute for Multidisciplinary Sciences) and Beate Veith (Department of Neurology, University Medical Center Göttingen) for their excellent technical assistance.

References

Adlkofer K, Frei R, Neuberg DHH, Zielasek J, Toyka K V & Suter U (1997) Heterozygous peripheral myelin protein 22-deficient mice are affected by a progressive demyelinating tomaculous neuropathy. *Journal of Neuroscience* 17: 4662–4671

Adlkofer K, Martini R, Aguzzi A, Zielasek J, Toyka K V. & Suter U (1995) Hypermyelination and demyelinating peripheral neuropathy in Pmp22-deficient mice. *Nat Genet* 11

Amici SA, Dunn WA, Murphy AJ, Adams NC, Gale NW, Valenzuela DM, Yancopoulos GD & Notterpek L (2006) Peripheral myelin protein 22 is in complex with α6β4 integrin, and its absence alters the Schwann cell basal lamina. *Journal of Neuroscience* 26

Ariotti N, Fernández-Rojo MA, Zhou Y, Hill MM, Rodkey TL, Inder KL, Tanner LB, Wenk MR, Hancock JF & Parton RG (2014) Caveolae regulate the nanoscale organization of the plasma membrane to remotely control Ras signaling. *Journal of Cell Biology* 204: 777–792

Arthur-Farraj P, Wanek K, Hantke J, Davis CM, Jayakar A, Parkinson DB, Mirsky R & Jessen KR (2011) Mouse schwann cells need both NRG1 and cyclic AMP to myelinate. *Glia* 59: 720–733

Azzaz F, Mazzarino M, Chahinian H, Yahi N, Scala C Di & Fantini J (2023) Structure of the Myelin Sheath Proteolipid Plasmolipin (PLLP) in a Ganglioside-Containing Lipid Raft. *Frontiers in Bioscience-Landmark* 28

Baechner D, Liehr T, Hameister H, Altenberger H, Grehl H, Suter U & Rautenstrauss B (1995) Widespread expression of the peripheral myelin protein-22 gene (pmp22) in neural and non-neural tissues during murine development. *J Neurosci Res* 42: 733–741

Bateman A, Martin M-J, Orchard S, Magrane M, Adesina A, Ahmad S, Bowler-Barnett EH, Bye-A-Jee H, Carpentier D, Denny P, *et al* (2025) UniProt: the Universal Protein Knowledgebase in 2025. *Nucleic Acids Res* 53: D609–D617

Benninger Y, Thurnherr T, Pereira JA, Krause S, Wu X, Chrostek-Grashoff A, Herzog D, Nave KA, Franklin RJM, Meijer D, *et al* (2007) Essential and distinct roles for cdc42 and rac1 in the regulation of Schwann cell biology during peripheral nervous system development. *Journal of Cell Biology* 177: 1051–1061

Bosse F, Hasse B, Pippirs U, Greiner-Petter R & Müller HW (2003) Proteolipid plasmolipin: Localization in polarized cells, regulated expression and lipid raft association in CNS and PNS myelin. *J Neurochem* 86: 508–518

Boutary S, Caillaud M, El Madani M, Vallat JM, Loisel-Duwattez J, Rouyer A, Richard L, Gracia C, Urbinati G, Desmaële D, *et al* (2021) Squalenoyl siRNA PMP22 nanoparticles are effective in treating mouse models of Charcot-Marie-Tooth disease type 1 A. *Commun Biol* 4

Boutary S, Khalaf G, Landesman Y, Madani M el, Desmaële D, Piguet F, Alonso R, Banchi EG, Adams D, Massaad C, *et al* (2025) Therapeutic potential of siRNA PMP22-SQ nanoparticles for Charcot-Marie-Tooth 1A neuropathy in rodents and non-human primates. *Int J Pharm* 671

Boutry J -M., Hauw J -J., Gansmüller A, Di-Bert N, Pouchelet M & Baron-Van Evercooren A (1992) Establishment and characterization of a mouse Schwann cell line which produces myelin in vivo. *J Neurosci Res* 32

Brancolini C, Marzinotto S, Edomi P, Agostoni E, Fiorentini C, Müller HW & Schneider C (1999) Rho-dependent regulation of cell spreading by the tetraspan membrane protein Gas3/PMP22. *Mol Biol Cell* 10

Brockes JP, Fields KL & Raff MC (1979) Studies on cultured rat Schwann cells. I. Establishment of purified populations from cultures of peripheral nerve. *Brain Res* 165: 105–18

Capodivento G, Camera M, Liessi N, Trada A, Debellis D, Schenone A, Armirotti A, Visigalli D & Nobbio L (2024) Monitoring Myelin Lipid Composition and the Structure of Myelinated Fibers Reveals a Maturation Delay in CMT1A. *Int J Mol Sci* 25

Chattopadhyay A & Harikumar KG (1996) Dependence of critical micelle concentration of a zwitterionic detergent on ionic strength: Implications in receptor solubilization. *FEBS Lett* 391: 199–202

Choy BC, Cater RJ, Mancia F & Pryor EE (2021) A 10-year meta-analysis of membrane protein structural biology: Detergents, membrane mimetics, and structure determination techniques. *Biochim Biophys Acta Biomembr* 1863

Chumakov I, Milet A, Cholet N, Primas G, Boucard A, Pereira Y, Graudens E, Mandel J, Laffaire J, Foucquier J, *et al* (2014) Polytherapy with a combination of three repurposed drugs (PXT3003) down-regulates Pmp22 over-expression and improves myelination, axonal and functional parameters in models of CMT1A neuropathy. *Orphanet J Rare Dis* 9: 1–16

Cox J & Mann M (2008) MaxQuant enables high peptide identification rates, individualized p.p.b.-range mass accuracies and proteome-wide protein quantification. *Nat Biotechnol* 26: 1367–1372

Dau T, Bartolomucci G & Rappsilber J (2020) Proteomics Using Protease Alternatives to Trypsin Benefits from Sequential Digestion with Trypsin. *Anal Chem* 92: 9523–9527

Deutsch EW, Bandeira N, Perez-Riverol Y, Sharma V, Carver JJ, Mendoza L, Kundu DJ, Wang S, Bandla C, Kamatchinathan S, *et al* (2023) The ProteomeXchange consortium at 10 years: 2023 update. *Nucleic Acids Res* 51: D1539–D1548

Dickson KM, Bergeron JJM, Shames I, Colby J, Nguyen DT, Chevet E, Thomas DY & Snipes GJ (2002) Association of calnexin with mutant peripheral myelin protein-22 ex vivo: a basis for ‘gain-of-function’ ER diseases. *Proc Natl Acad Sci U S A* 99

Dittmer TA, Sahni N, Kubben N, Hill DE, Vidal M, Burgess RC, Roukos V & Misteli T (2014) Systematic identification of pathological lamin A interactors. *Mol Biol Cell* 25: 1493–1510

Dunham WH, Mullin M & Gingras A (2012) Affinity-purification coupled to mass spectrometry: Basic principles and strategies. *Proteomics* 12: 1576–1590

D’Urso D, Ehrhardt P & Müller HW (1999) Peripheral Myelin Protein 22 and Protein Zero: a Novel Association in Peripheral Nervous System Myelin. *The Journal of Neuroscience* 19

Dzwonek J & Wilczyński GM (2015) CD44: Molecular interactions, signaling and functions in the nervous system. *Front Cell Neurosci* 9

Espallergues J, Cadiet J, Souab F, Choquet O, Swisser F, Bigeleisen P, Maleysson V, Sola M-L, van Hameren G & Tricaud N (2025) Perineural delivery of AAV2/9 in non-human primate is a

safe and efficient route for gene therapy in Charcot-Marie-Tooth diseases. *Mol Ther Methods Clin Dev*: 101548

Feng Z, Fang P, Zheng H & Zhang X (2023) DEP2: an upgraded comprehensive analysis toolkit for quantitative proteomics data. *Bioinformatics* 39

Fischer F & Poetsch A (2006) Protein cleavage strategies for an improved analysis of the membrane proteome. *Proteome Sci* 4

Fledrich R, Abdelaal T, Rasch L, Bansal V, Schütza V, Brügger B, Lüchtenborg C, Prukop T, Stenzel J, Rahman RU, *et al* (2018) Targeting myelin lipid metabolism as a potential therapeutic strategy in a model of CMT1A neuropathy. *Nat Commun* 9

Fledrich R, Akkermann D, Schütza V, Abdelaal TA, Hermes D, Schäffner E, Soto-Bernardini MC, Götze T, Klink A, Kusch K, *et al* (2019) NRG1 type I dependent autoparacrine stimulation of Schwann cells in onion bulbs of peripheral neuropathies. *Nat Commun* 10

Fledrich R, Schlotter-Weigel B, Schnizer TJ, Wichert SP, Stassart RM, Meyer zu Hörste G, Klink A, Weiss BG, Haag U, Walter MC, *et al* (2012) A rat model of Charcot–Marie–Tooth disease 1A recapitulates disease variability and supplies biomarkers of axonal loss in patients. *Brain* 135

Fledrich R, Stassart RM, Klink A, Rasch LM, Prukop T, Haag L, Czesnik D, Kungl T, Abdelaal TAM, Keric N, *et al* (2014) Soluble neuregulin-1 modulates disease pathogenesis in rodent models of Charcot-Marie-Tooth disease 1A. *Nat Med* 20

Fontanini A, Chies R, Snapp EL, Ferrarini M, Fabrizi GM & Brancolini C (2005) Glycan-independent role of calnexin in the intracellular retention of Charcot-Marie-Tooth 1IA Gas3/PMP22 mutants. *Journal of Biological Chemistry* 280: 2378–2387

Fornasari BE, Ronchi G, Pascal D, Visigalli D, Capodivento G, Nobbio L, Perroteau I, Schenone A, Geuna S & Gambarotta G (2018) Soluble Neuregulin1 is strongly up-regulated in the rat model of Charcot-Marie-Tooth 1A disease. *Exp Biol Med* 243: 370–374

Furuse M, Fujita K, Hiiragi T, Fujimoto K & Tsukita S (1998) Claudin-1 and -2: Novel Integral Membrane Proteins Localizing at Tight Junctions with No Sequence Similarity to Occludin. *J Cell Biol* 141: 1539–1550

Gautier B, Hajjar H, Soares S, Berthelot J, Deck M, Abbou S, Campbell G, Ceprian M, Gonzalez S, Fovet CM, *et al* (2021) AAV2/9-mediated silencing of PMP22 prevents the development of pathological features in a rat model of Charcot-Marie-Tooth disease 1 A. *Nat Commun* 12

Gitik M, Liraz-Zaltsman S, Oldenborg PA, Reichert F & Rotshenker S (2011) Myelin down-regulates myelin phagocytosis by microglia and macrophages through interactions between CD47 on myelin and SIRPα (signal regulatory protein-α) on phagocytes. *J Neuroinflammation* 8

Götzke H, Kilisch M, Martínez-Carranza M, Sograte-Idrissi S, Rajavel A, Schlichthaerle T, Engels N, Jungmann R, Stenmark P, Opazo F, *et al* (2019) The ALFA-tag is a highly versatile tool for nanobody-based bioscience applications. *Nat Commun* 10

Guo J, Wang L, Zhang Y, Wu J, Arpag S, Hu B, Imhof BA, Tian X, Carter BD, Suter U, *et al* (2014) Abnormal junctions and permeability of myelin in PMP22-deficient nerves. *Ann Neurol* 75: 255–265

Haenig C, Atias N, Taylor AK, Mazza A, Schaefer MH, Russ J, Riechers SP, Jain S, Coughlin M, Fontaine JF, *et al* (2020) Interactome Mapping Provides a Network of Neurodegenerative Disease Proteins and Uncovers Widespread Protein Aggregation in Affected Brains. *Cell Rep* 32

Hanemann CO, D'Urso D, Gabreëls-Festen AAWM & Müller HW (2000) Mutation-dependent alteration in cellular distribution of peripheral myelin protein 22 in nerve biopsies from Charcot–Marie–Tooth type 1A. *Brain* 123

Hara T, Hashimoto Y, Akuzawa T, Hirai R, Kobayashi H & Sato K (2014) Rer1 and calnexin regulate endoplasmic reticulum retention of a peripheral myelin protein 22 mutant that causes type 1A Charcot-Marie-Tooth disease. 22

Harrison PJ, Vecerkova T, Clare DK & Quigley A (2023) A review of the approaches used to solve sub-100 kDa membrane proteins by cryo-electron microscopy. *J Struct Biol* 215

Hayashi A, Nakashima K, Yamagishi K, Hoshi T, Suzuki A & Baba H (2007) Localization of annexin II in the paranodal regions and Schmidt–Lanterman incisures in the peripheral nervous system. *Glia* 55: 1044–1052

Hertzog N & Jacob C (2023) Mechanisms and treatment strategies of demyelinating and dysmyelinating Charcot-Marie-Tooth disease. *Neural Regen Res* 18: 1931–1939

Hu B, Arpag S, Zhang X, Möbius W, Werner HB, Sosinsky G, Ellisman M, Zhang Y, Hamilton A, Chernoff J, *et al* (2016) Tuning PAK Activity to Rescue Abnormal Myelin Permeability in HNPP. *PLoS Genet* 12

Huang DW, Sherman BT & Lempicki RA (2009) Systematic and integrative analysis of large gene lists using DAVID bioinformatics resources. *Nat Protoc* 4: 44–57

Hughes CS, Moggridge S, Müller T, Sorensen PH, Morin GB & Krijgsveld J (2019) Single-pot, solid-phase-enhanced sample preparation for proteomics experiments. *Nat Protoc* 14: 68–85

Jouaud M, Mathis S, Richard L, Lia A-S, Magy L & Vallat J-M (2019) Rodent models with expression of PMP22: Relevance to dysmyelinating CMT and HNPP. *J Neurol Sci* 398

Kim M, Wende H, Walcher J, Küehnemund J, Cheret C, Kempa S, McShane E, Selbach M, Lewin GR & Birchmeier C (2018) Maf links neuregulin1 signaling to cholesterol synthesis in myelinating schwann cells. *Genes Dev* 32: 645–657

Kitamura K, Suzuki M & Uyemura K (1976) Purification and partial characterization of two glycoproteins in bovine peripheral nerve myelin membrane. *BBA - Biomembranes* 455: 806–816

Krauter D, Stausberg D, Hartmann TJ, Volkmann S, Kungl T, Rasche DA, Saher G, Fledrich R, Stassart RM, Nave K-A, *et al* (2024) Targeting PI3K/Akt/mTOR signaling in rodent models of PMP22 gene-dosage diseases. *EMBO Mol Med* 16

Labeta MO, Fernandez N & Festenstein H (1988) Solubilisation effect of Nonidet P-40, Triton X-100 and CHAPS in the detection of MHC-like glycoproteins

Larance M, Kirkwood KJ, Tinti M, Murillo AB, Ferguson MAJ & Lamond AI (2016) Global membrane protein interactome analysis using in vivo crosslinking and mass spectrometry-based protein correlation profiling. *Molecular and Cellular Proteomics* 15: 2476–2490

LeBlanc SE, Srinivasan R, Ferri C, Mager GM, Gillian-Daniel AL, Wrabetz L & Svaren J (2005) Regulation of cholesterol/lipid biosynthetic genes by Egr2/Krox20 during peripheral nerve myelination. *J Neurochem* 93: 737–748

Leitner A, Faini M, Stengel F & Aebersold R (2016) Crosslinking and Mass Spectrometry: An Integrated Technology to Understand the Structure and Function of Molecular Machines. *Trends Biochem Sci* 41: 20–32

Van Lent J, Vendredy L, Adriaenssens E, Da Silva Authier T, Asselbergh B, Kaji M, Weckhuysen S, Van Den Bosch L, Baets J & Timmerman V (2023) Downregulation of PMP22 ameliorates myelin defects in iPSC-derived human organoid cultures of CMT1A. *Brain* 146: 2885–2896

Li J, Parker B, Martyn C, Natarajan C & Guo J (2013) The PMP22 Gene and Its Related Diseases. *Mol Neurobiol* 47

Li S, Xie T, Liu P, Wang L & Gong X (2021) Structural insights into the assembly and substrate selectivity of human SPT–ORMDL3 complex. *Nat Struct Mol Biol* 28: 249–257

Lin YC, Boone M, Meuris L, Lemmens I, Van Roy N, Soete A, Reumers J, Moisse M, Plaisance S, Drmanac R, *et al* (2014) Genome dynamics of the human embryonic kidney 293 lineage in response to cell biology manipulations. *Nat Commun* 5

Liu S & Chen Z (2015) The Functional Role of PMP22 Gene in the Proliferation and Invasion of Osteosarcoma. *Med Sci Monit* 21: 1976–82

Luck K, Kim DK, Lambourne L, Spirohn K, Begg BE, Bian W, Brignall R, Cafarelli T, Campos-Laborie FJ, Charloteaux B, *et al* (2020) A reference map of the human binary protein interactome. *Nature* 580: 402–408

Lupski JR, de Oca-Luna RM, Slaugenhaupt S, Pentao L, Guzzetta V, Trask BJ, Saucedo-Cardenas O, Barker DF, Killian JM, Garcia CA, *et al* (1991) DNA duplication associated with Charcot-Marie-Tooth disease type 1A. *Cell* 66: 219–232

Lupski JR, Wise CA, Kuwano A, Pentao L, Parke JT, Glaze DG, Ledbetter DH, Greenberg F & Patel PI (1992) Gene dosage is a mechanism for Charcot-Marie-Tooth disease type 1A. *Nat Genet* 1: 29–33

Machleidt T, Woodroofe CC, Schwinn MK, Méndez J, Robers MB, Zimmerman K, Otto P, Daniels DL, Kirkland TA & Wood K V. (2015) NanoBRET-A Novel BRET Platform for the Analysis of Protein-Protein Interactions. *ACS Chem Biol* 10: 1797–1804

Marinko JT, Carter BD & Sanders CR (2020) Direct relationship between increased expression and mistrafficking of the Charcot-Marie-Tooth-associated protein PMP22. *Journal of Biological Chemistry* 295: 11963–11970

Marinko JT, Wright MT, Schlebach JP, Clowes KR, Heintzman DR, Plate L & Sanders CR (2021) Glycosylation limits forward trafficking of the tetraspan membrane protein PMP22. *Journal of Biological Chemistry* 296

Matsunami N, Smith3 B, Ballard2 L, Lensch3 MW, Robertson M, Albertsen H, Hanemann\ CO, Miiller4 HW, Bird5 TD, White R, *et al* (1992) Peripheral myelin protein-22 gene maps in the duplication in chromosome 17p11.2 associated with Charcot-Marie-Tooth 1A

Meyer zu Hörste G, Prukop T, Liebetanz D, Möbius W, Nave KA & Sereda MW (2007) Antiprogesterone therapy uncouples axonal loss from demyelination in a transgenic rat model of CMT1A neuropathy. *Ann Neurol* 61: 61–72

Michaelis AC, Brunner AD, Zwiebel M, Meier F, Strauss MT, Bludau I & Mann M (2023) The social and structural architecture of the yeast protein interactome. *Nature* 624: 192–200

Michailidou I, Vreijling J, Rumpf M, Loos M, Koopmans B, Vlek N, Straat N, Agaser C, Kuipers TB, Mei H, *et al* (2023) The systemic inhibition of the terminal complement system reduces neuroinflammation but does not improve motor function in mouse models of CMT1A with overexpressed PMP22. *Current Research in Neurobiology* 4

Mobley CK, Myers JK, Hadziselimovic A, Ellis CD & Sanders CR (2007) Purification and initiation of structural characterization of human peripheral myelin protein 22, an integral membrane protein linked to peripheral neuropathies. *Biochemistry* 46

Newstead S, Ferrandon S & Iwata S (2008) Rationalizing α-helical membrane protein crystallization. *Protein Science* 17: 466–472

Niemann S, Sereda MW, Suter U, Griffiths IR & Nave KA (2000) Uncoupling of myelin assembly and schwann cell differentiation by transgenic overexpression of peripheral myelin protein 22. *J Neurosci* 20: 4120–8

Nishimura T, Yoshikawa H, Fujimura H, Sakoda S & Yanagihara T (1996) Accumulation of peripheral myelin protein 22 in onion bulbs and Schwann cells of biopsied nerves from patients with Charcot-Marie-Tooth disease type 1A. *Acta Neuropathol* 92

Notterpek L, Roux KJ, Amici SA, Yazdanpour A, Rahner C & Fletcher BS (2001) Peripheral myelin protein 22 is a constituent of intercellular junctions in epithelia. *Proceedings of the National Academy of Sciences* 98

O'Reilly FJ & Rappsilber J (2018) Cross-linking mass spectrometry: methods and applications in structural, molecular and systems biology. *Nat Struct Mol Biol* 25: 1000–1008

Örtegren U, Karlsson M, Blazic N, Blomqvist M, Nystrom FH, Gustavsson J, Fredman P & Strålfors P (2004) Lipids and glycosphingolipids in caveolae and surrounding plasma membrane of primary rat adipocytes. *Eur J Biochem* 271

Pareyson D & Marchesi C (2009) Diagnosis, natural history, and management of Charcot–Marie–Tooth disease. *Lancet Neurol* 8

Pashkova N, Peterson TA, Ptak CP, Winistorfer SC, Guerrero-Given D, Kamasawa N, Ahern CA, Shy ME & Piper RC (2024) Disrupting the transmembrane domain interface between PMP22 and MPZ causes peripheral neuropathy. *iScience* 27

Patel PI, Roa BB, Welcher AA, Schoener-Scott R, Trask BJ, Pentao L, Jackson Snipes G, Garcia CA, Francke U, Shooter EM, *et al* (1992) The gene for the peripheral myelin protein PMP-22 is a candidate for Charcot-Marie-Tooth disease type 1A

Pertusa M, Morenilla-Palao C, Carteron C, Viana F & Cabedo H (2007) Transcriptional control of cholesterol biosynthesis in schwann cells by axonal neuregulin 1. *Journal of Biological Chemistry* 282: 28768–28778

Piersimoni L, Kastritis PL, Arlt C & Sinz A (2022) Cross-Linking Mass Spectrometry for Investigating Protein Conformations and Protein–Protein Interactions—A Method for All Seasons. *Chem Rev* 122: 7500–7531

Pisciotta C & Shy ME (2023) Hereditary neuropathy. In *Handbook of clinical neurology* pp 609–617.

Poitelon Y, Kopec AM & Belin S (2020) Myelin Fat Facts: An Overview of Lipids and Fatty Acid Metabolism. *Cells* 9: 812

Poitelon Y, Matafora V, Silvestri N, Zambroni D, McGarry C, Serghany N, Rush T, Vizzuso D, Court FA, Bachi A, *et al* (2018) A dual role for Integrin α6β4 in modulating hereditary neuropathy with liability to pressure palsies. *J Neurochem* 145: 245–257

Prior R, Silva A, Vangansewinkel T, Idkowiak J, Tharkeshwar AK, Hellings TP, Michailidou I, Vreijling J, Loos M, Koopmans B, *et al* (2024) PMP22 duplication dysregulates lipid homeostasis and plasma membrane organization in developing human Schwann cells. *Brain*

Prukop T, Stenzel J, Wernick S, Kungl T, Mroczek M, Adam J, Ewers D, Nabirotchkin S, Nave K-A, Hajj R, *et al* (2019) Early short-term PXT3003 combinational therapy delays disease onset in a transgenic rat model of Charcot-Marie-Tooth disease 1A (CMT1A). *PLoS One* 14

Prukop T, Wernick S, Boussicault L, Ewers D, Jäger K, Adam J, Winter L, Quintes S, Linhoff L, Barrantes-Freer A, *et al* (2020) Synergistic PXT3003 therapy uncouples neuromuscular function from dysmyelination in male Charcot–Marie–Tooth disease type 1A (CMT1A) rats. *J Neurosci Res* 98

Puiu M & Bala C (2016) SPR and SPR Imaging: Recent Trends in Developing Nanodevices for Detection and Real-Time Monitoring of Biomolecular Events. *Sensors* 16: 870

Qu H, Zhu M, Tao Y & Zhao Y (2015) Suppression of peripheral myelin protein 22 (PMP22) expression by miR29 inhibits the progression of lung cancer. *Neoplasma* 62: 881–6

Quinville BM, Deschenes NM, Ryckman AE & Walia JS (2021) A Comprehensive Review: Sphingolipid Metabolism and Implications of Disruption in Sphingolipid Homeostasis. *Int J Mol Sci* 22: 5793

Raeymaekers P, Timmerman V, Nelis E, De Jonghe P, Hoogenduk JE, Baas F, Barker DF, Martin JJ, De Visser M, Bolhuis PA, *et al* (1991) Duplication in chromosome 17p11.2 in Charcot-Marie-Tooth neuropathy type 1a (CMT 1a). *Neuromuscular Disorders* 1: 93–97

Rao RG, Sudhakar D, Hogue CP, Amici S, Gordon LK, Braun J, Notterpek L, Goodglick L & Wadehra M (2011) Peripheral myelin protein-22 (PMP22) modulates alpha 6 integrin expression in the human endometrium. *Reproductive Biology and Endocrinology* 9

Reed M, Luissint AC, Azcutia V, Fan S, O'Leary MN, Quiros M, Brazil J, Nusrat A & Parkos CA (2019) Epithelial CD47 is critical for mucosal repair in the murine intestine in vivo. *Nat Commun* 10

Rolland T, Taşan M, Charloteaux B, Pevzner SJ, Zhong Q, Sahni N, Yi S, Lemmens I, Fontanillo C, Mosca R, *et al* (2014) A proteome-scale map of the human interactome network. *Cell* 159: 1212–1226

Roux KJ, Amici SA, Fletcher BS & Notterpek L (2005) Modulation of Epithelial Morphology, Monolayer Permeability, and Cell Migration by Growth Arrest Specific 3/Peripheral Myelin Protein 22. *Mol Biol Cell* 16

Roux KJ, Amici SA & Notterpek L (2004) The temporospatial expression of peripheral myelin protein 22 at the developing blood-nerve and blood-brain barriers. *Journal of Comparative Neurology* 474

Russell WC, Graham FL, Smiley J & Nairn R (1977) Characteristics of a Human Cell Line Transformed by DNA from Human Adenovirus Type 5. *Journal of General Virology* 36: 59–72

Sahni N, Yi S, Taipale M, Fuxman Bass JI, Coulombe-Huntington J, Yang F, Peng J, Weile J, Karras GI, Wang Y, *et al* (2015) Widespread macromolecular interaction perturbations in human genetic disorders. *Cell* 161: 647–660

Schneider C, King RM & Philipson L (1988) Genes specifically expressed at growth arrest of mammalian cells. *Cell* 54

Sereda M, Griffiths I, Pühlhofer A, Stewart H, Rossner MJ, Zimmermann F, Magyar JP, Schneider A, Hund E, Meinck H-M, *et al* (1996) A Transgenic Rat Model of Charcot-Marie-Tooth Disease. *Neuron* 16: 1049–1060

Sereda MW, Meyer zu Hörste G, Suter U, Uzma N & Nave K-A (2003) Therapeutic administration of progesterone antagonist in a model of Charcot-Marie-Tooth disease (CMT-1A). *Nat Med* 9

Serfecz J, Bazick H, Al Salihi MO, Turner P, Fields C, Cruz P, Renne R & Notterpek L (2019) Downregulation of the human peripheral myelin protein 22 gene by miR-29a in cellular models of Charcot–Marie–Tooth disease. *Gene Ther* 26: 455–464

Sharifi Tabar M, Parsania C, Chen H, Su X-D, Bailey CG & Rasko JEJ (2022) Illuminating the dark protein-protein interactome. *Cell Reports Methods* 2: 100275

Shaw G, Morse S, Ararat M & Graham FL (2002) Preferential transformation of human neuronal cells by human adenoviruses and the origin of HEK 293 cells. *The FASEB journal : official publication of the Federation of American Societies for Experimental Biology* 16: 869–871

Sherman BT, Hao M, Qiu J, Jiao X, Baseler MW, Lane HC, Imamichi T & Chang W (2022) DAVID: a web server for functional enrichment analysis and functional annotation of gene lists (2021 update). *Nucleic Acids Res* 50: W216–W221

Shevchenko A, Wilm M, Vorm O & Mann M (1996) Mass Spectrometric Sequencing of Proteins from Silver-Stained Polyacrylamide Gels. *Anal Chem* 68: 850–858

Shih IM, Nesbit M, Herlyn M & Kurman RJ (1998) A new Mel-CAM (CD146)-specific monoclonal antibody, MN-4, on paraffin-embedded tissue. *Mod Pathol* 11: 1098–106

Siems SB, Jahn O, Eichel MA, Kannaiyan N, Wu LMN, Sherman DL, Kusch K, Hesse D, Jung RB, Fledrich R, *et al* (2020) Proteome profile of peripheral myelin in healthy mice and in a neuropathy model. *Elife* 9

Silva A, Prior R, D'Antonio M, Swinnen J V. & Van Den Bosch L (2025) Lipid metabolism alterations in peripheral neuropathies. *Neuron* 113: 2556–2581

Snipes GJ, Suter U, Welcher AA & Shooter E ric M (1992) Characterization of a novel peripheral nervous system myelin protein (PMP- 22/SR13). *Journal of Cell Biology* 117: 225–238

Söderberg O, Gullberg M, Jarvius M, Ridderstråle K, Leuchowius KJ, Jarvius J, Wester K, Hydbring P, Bahram F, Larsson LG, *et al* (2006) Direct observation of individual endogenous protein complexes in situ by proximity ligation. *Nat Methods* 3: 995–1000

Stefanski KM, Wilkinson MC & Sanders CR (2024) Roles for PMP22 in Schwann cell cholesterol homeostasis in health and disease. *Biochem Soc Trans* 52: 1747–1756

Stetsenko A & Guskov A (2017) An overview of the top ten detergents used for membrane protein crystallization. *Crystals (Basel)* 7

Stumpf MPH, Thorne T, de Silva E, Stewart R, An HJ, Lappe M & Wiuf C (2008) Estimating the size of the human interactome. *Proceedings of the National Academy of Sciences* 105: 6959–6964

Subach OM, Cranfill PJ, Davidson MW & Verkhusha V V. (2011) An enhanced monomeric blue fluorescent protein with the high chemical stability of the chromophore. *PLoS One* 6

Suter U, Snipes GJ, Schoener-Scott R, Welcher AA, Pareek S, Lupski JR, Murphy RA, Shooter EM & Patel PI (1994) Regulation of tissue-specific expression of alternative peripheral myelin protein-22 (PMP22) gene transcripts by two promoters. *Journal of Biological Chemistry* 269: 25795–25808

Timmerman V, Nelis E, Van Hul W, Nieuwenhuijsen BW, Chen KL, Wang S, Othman K Ben, Cullen B, Leach RJ, Hanemann CO, *et al* (1992) The peripheral myelin protein gene PMP–22 is contained within the Charcot–Marie–Tooth disease type 1A duplication. *Nat Genet* 1: 171–175

Tobler AR, Notterpek L, Naef R, Taylor V, Suter U & Shooter EM (1999) Transport of *Trembler-J* Mutant Peripheral Myelin Protein 22 Is Blocked in the Intermediate Compartment and Affects the Transport of the Wild-Type Protein by Direct Interaction. *The Journal of Neuroscience* 19

Vagin O, Tokhtaeva E & Sachs G (2006) The role of the β1 subunit of the Na,K-ATPase and its glycosylation in cell-cell adhesion. *Journal of Biological Chemistry* 281: 39573–39587

Valentijn LJ, Bolhuis1 PA, Zorn I, Hoogendijk1 JE, Van Den Bosch1 N, Hensels1 GW, Stanton VP, Housman2 DE, Fischbeck3 KH, Ross4 DA, *et al* (1992) The peripheral myelin gene PMP-22/GAS-3 is duplicated in Charcot-Marie-Tooth disease type1A

Vanoye CG, Sakakura M, Follis RM, Trevisan AJ, Narayan M, Li J, Sanders CR & Carter BD (2019) Peripheral myelin protein 22 modulates store-operated calcium channel activity, providing insights into Charcot-Marie-Tooth disease etiology. *Journal of Biological Chemistry* 294

Vénien-Bryan C & Fernandes CAH (2023) Overview of Membrane Protein Sample Preparation for Single-Particle Cryo-Electron Microscopy Analysis. *Int J Mol Sci* 24: 14785

Venkatesan K, Rual JF, Vazquez A, Stelzl U, Lemmens I, Hirozane-Kishikawa T, Hao T, Zenkner M, Xin X, Goh K II, *et al* (2009) An empirical framework for binary interactome mapping. *Nat Methods* 6: 83–90

Vigo T, Nobbio L, Van Hummelen P, Abbruzzese M, Mancardi G, Verpoorten N, Verhoeven K, Sereda MW, Nave KA, Timmerman V, *et al* (2005) Experimental Charcot-Marie-Tooth type 1A: A cDNA microarrays analysis. *Molecular and Cellular Neuroscience* 28: 703–714

Visigalli D, Capodivento G, Basit A, Fernández R, Hamid Z, Pencová B, Gemelli C, Marubbi D, Pastorino C, Luoma AM, *et al* (2020) Exploiting Sphingo- and Glycerophospholipid Impairment to Select Effective Drugs and Biomarkers for CMT1A. *Front Neurol* 11

Wang J, Huo K, Ma L, Tang L, Li D, Huang X, Yuan Y, Li C, Wang W, Guan W, *et al* (2011) Toward an understanding of the protein interaction network of the human liver. *Mol Syst Biol* 7

Wang X-Q, Lindberg FP & Frazier WA (1999) Integrin-associated Protein Stimulates 2 1-dependent Chemotaxis via Gi-mediated Inhibition of Adenylate Cyclase and Extracellular-regulated Kinases

Wang XW, Madeddu L, Spirohn K, Martini L, Fazzone A, Becchetti L, Wytock TP, Kovács IA, Balogh OM, Benczik B, *et al* (2023) Assessment of community efforts to advance network-based prediction of protein–protein interactions. *Nat Commun* 14

Wang Y, Niu Y, Zhang Z, Gable K, Gupta SD, Somashekarappa N, Han G, Zhao H, Myasnikov AG, Kalathur RC, *et al* (2021) Structural insights into the regulation of human serine palmitoyltransferase complexes. *Nat Struct Mol Biol* 28: 240–248

Wilson HL, Wilson SA, Surprenant A & North RA (2002) Epithelial Membrane Proteins Induce Membrane Blebbing and Interact with the P2X 7 Receptor C Terminus *. 277: 34017–34023

Winslow S, Leandersson K & Larsson C (2013) Regulation of PMP22 mRNA by G3BP1 affects cell proliferation in breast cancer cells. *Mol Cancer* 12: 156

Yaffe Y, Hugger I, Yassaf IN, Shepshelovitch J, Sklan EH, Elkabetz Y, Yeheskel A, Pasmanik-Chor M, Benzing C, Macmillan A, *et al* (2015) The myelin proteolipid plasmolipin forms oligomers and induces liquid-ordered membranes in the Golgi complex. *J Cell Sci* 128: 2293–2302

Yoshioka Y, Taniguchi JB, Homma H, Tamura T, Fujita K, Inotsume M, Tagawa K, Misawa K, Matsumoto N, Nakagawa M, *et al* (2023) AAV-mediated editing of PMP22 rescues Charcot-Marie-Tooth disease type 1A features in patient-derived iPS Schwann cells. *Communications Medicine* 3

Zanotti A, Coelho JPL, Kaylani D, Singh G, Tauber M, Hitzenberger M, Avci D, Zacharias M, Russell RB, Lemberg MK, *et al* (2022) The human signal peptidase complex acts as a quality control enzyme for membrane proteins. *Science (1979)* 378

Zhao HT, Damle S, Ikeda-Lee K, Kuntz S, Li J, Mohan A, Kim A, Hung G, Scheideler MA, Scherer SS, *et al* (2018) PMP22 antisense oligonucleotides reverse Charcot-Marie-Tooth disease type 1A features in rodent models. *Journal of Clinical Investigation* 128: 359–368

Zhou Y, Borchelt D, Bauson JC, Fazio S, Miles JR, Tavori H & Notterpek L (2020) Subcellular diversion of cholesterol by gain- and loss-of-function mutations in PMP22. *Glia* 68: 2300–2315

Zhou Y, Miles JR, Tavori H, Lin M, Khoshbouei H, Borchelt DR, Bazick H, Landreth GE, Lee S, Fazio S, *et al* (2019) PMP22 regulates cholesterol trafficking and ABCA1-mediated cholesterol efflux. *Journal of Neuroscience* 39

Zoltewicz SJ, Lee S, Chittoor VG, Freeland SM, Rangaraju S, Zacharias DA & Notterpek L (2012) The palmitoylation state of PMP22 modulates epithelial cell morphology and migration. *ASN Neuro* 4